

scientific reports



OPEN

Cyclin M2 (CNNM2) knockout mice show mild hypomagnesaemia and developmental defects

Gijs A. C. Franken^{1,5}, Murat Seker^{2,5}, Caro Bos¹, Laura A. H. Siemons¹,
Bram C. J. van der Eerden³, Annabel Christ⁴, Joost G. J. Hoenderop¹, René J. M. Bindels¹,
Dominik Müller², Tilman Breiderhoff² & Jeroen H. F. de Baaij¹✉

Patients with mutations in Cyclin M2 (CNNM2) suffer from hypomagnesaemia, seizures, and intellectual disability. Although the molecular function of CNNM2 is under debate, the protein is considered essential for renal Mg²⁺ reabsorption. Here, we used a *Cnnm2* knock out mouse model, generated by CRISPR/Cas9 technology, to assess the role of CNNM2 in Mg²⁺ homeostasis. Breeding *Cnnm2*^{-/-} mice resulted in a Mendelian distribution at embryonic day 18. Nevertheless, only four *Cnnm2*^{-/-} pups were born alive. The *Cnnm2*^{-/-} pups had a significantly lower serum Mg²⁺ concentration compared to wildtype littermates. Subsequently, adult *Cnnm2*^{-/-} mice were fed with low, control, or high Mg²⁺ diets for two weeks. Adult *Cnnm2*^{-/-} mice showed mild hypomagnesaemia compared to *Cnnm2*^{+/+} mice and increased serum Ca²⁺ levels, independent of dietary Mg²⁺ intake. Faecal analysis displayed increased Mg²⁺ and Ca²⁺ excretion in the *Cnnm2*^{-/-} mice. Transcriptional profiling of *Trpm6*, *Trpm7*, and *Slc41a1* in kidneys and colon did not reveal effects based on genotype. Microcomputed tomography analysis of the femurs demonstrated equal bone morphology and density. In conclusion, CNNM2 is vital for embryonic development and Mg²⁺ homeostasis. Our data suggest a previously undescribed role of CNNM2 in the intestine, which may contribute to the Mg²⁺ deficiency in mice and patients.

Hypomagnesaemia is defined by a serum magnesium (Mg²⁺) level below <0.7 mmol/L and is associated with hypertension, muscle cramps, diabetes mellitus type II, epilepsy, and cardiac arrhythmias¹. To maintain a physiological blood Mg²⁺ concentration, the intestine absorbs Mg²⁺ from the diet and can subsequently be stored in soft tissues and bone. The kidneys are considered as major regulators of the blood Mg²⁺ concentration. Here, Mg²⁺ is largely reabsorbed via paracellular transport in the proximal tubule and thick ascending limb of Henle (TAL). Fine-tuning of Mg²⁺ reabsorption take place in the distal convoluted tubule (DCT), where transport is an active transcellular process².

In the DCT, apical Mg²⁺ transport is realised by the luminal divalent cation channel transient receptor potential melastatin type 6 and 7 (TRPM6/7)³⁻⁷. Mutations in TRPM6 cause hypomagnesaemia with secondary hypocalcaemia (HOMG1/HSH; MIM# 602014). At the basolateral side, several proteins have been considered to facilitate Mg²⁺ extrusion including solute carrier 41a1 (SLC41A1) and Cyclin M2 (CNNM2)⁸. Although the definite role of this latter protein has not been elucidated on a molecular level, patient studies have shown the importance of CNNM2 in renal Mg²⁺ handling⁸⁻¹¹. Mutations in this gene are causative for hypomagnesaemia, seizures, and intellectual disability (HSMR) syndrome (HSMR; MIM# 616418)¹²⁻¹⁴. In addition to renal Mg²⁺ wasting, patients suffer from seizures, motor skills difficulties, intellectual disability, and deficits in speech^{12,13}. Only patients affected by recessive mutations have been demonstrated to show structural brain anomalies, such as demyelination or enlarged supratentorial outer cerebrospinal liquor spaces¹³. Of note, genome wide associates studies (GWAS) have linked the *CNNM2* locus with grey matter morphology, schizophrenia, increased body mass index, and hypertension¹⁵⁻¹⁹.

¹Department of Physiology, Radboud Institute for Molecular Life Sciences, Radboud University Medical Center, P.O. Box 9101, 6500HB Nijmegen, The Netherlands. ²Department of Pediatric Gastroenterology, Nephrology and Metabolic Diseases, Charité – Universitätsmedizin Berlin, Berlin, Germany. ³Department of Internal Medicine, Erasmus Medical Center, Rotterdam, The Netherlands. ⁴Department of Molecular Cardiovascular Research, Max-Delbrueck-Center for Molecular Medicine, Berlin, Germany. ⁵These authors contributed equally: Gijs A. C. Franken and Murat Seker. ✉email: jeroen.debaaij@radboudumc.nl

Although CNNM2 plays an important role in renal Mg^{2+} homeostasis and brain function, the underlying molecular mechanisms and their implications for patients suffering from HSMR syndrome have not been elucidated. Therefore, the aim of this study was to investigate the role of CNNM2-mediated Mg^{2+} homeostasis in greater detail by generating novel CNNM2 mouse models.

Methods

Generation of CNNM2 deficient mice. *Cnnm2*^{-/-} mice were generated by CRISPR/Cas9 mediated genomic editing in murine zygotes²⁰. In brief, guide RNAs were cloned into pX330 (pX330 was a gift from Feng Zhang (Addgene plasmid 42230) and Cas9 into pTLN²¹. For the generation of Indels in *Cnnm2* the target sequence was 5'-GTCCTGCAAGCAGCTGCGGGC-3', for insertion of the loxP sites 5'-CTGTAGTAGATCCTCGCGC-3' and 5'-GCATCCCGCAGGGTAGATTA-3'. A T7-promoter was added to the sgRNA sequence by PCR and the Cas9 plasmid was linearized using MluI. The PCR product and the linearized plasmid were in vitro transcribed using MEGA shortscript and mMessage Machine KIT (Life Technologies, United States of America (USA)). Both Cas9 mRNA and the sgRNAs were purified using MEGAclean kit (Life Technologies) and eluted in RNase-free water. For the generation of the Indel allele, Cas9 mRNA and sgRNA, for the generation of the floxed allele *Cas9* mRNA, sgRNAs and a plasmid containing a floxed exon 1 of *Cnnm2* were injected into fertilized zygotes. These zygotes were kept overnight (O/N) at 37 °C and then transferred to pseudopregnant foster mice. Founders were identified by PCR and Sanger sequencing. Mice were bred to C57Bl/6N for two generations. The deleted allele was obtained by crossing mice with the floxed allele to a Cre deleter strain (Tg(CMV-cre)1Cgn; JAX #006054).

Animals and ethics. Two animal studies were performed: a study with embryos and newborn with both *Cnnm2*^{+/+}, *Cnnm2*^{+/-} and *Cnnm2*^{-/-} mice and was performed in Charité, Berlin. The other study was performed in the Radboud Institute for Molecular Life Sciences, Nijmegen and used 30 *Cnnm2*^{+/+} mice (15 female, 15 male) and 36 *Cnnm2*^{+/-} mice (18 female, 18 male). These mice subsequently divided over three experimental groups (*Cnnm2*^{+/+} 10 per group, 5 male/female and *Cnnm2*^{+/-} 16 mice per group, 6 male/female).

Mice were maintained according to institutional guidelines of Charité Berlin. After timed mating of the mothers, embryos were isolated on day 18.5 of gestation. Newborns were culled directly after birth. Genotyping of the allele containing the deletion was performed using the oligonucleotides 5'-CCGGGTGGGAAGGATGAAGC-3' and 5'-GGGACCACGTCTCGTTGTG-3', and of the floxed allele using the oligonucleotides 5'-AGTCCGGCTCTGGTGCTC-3' (KO), 5'-AAGCCAAAACCTGCCATTAC-3' (WT), 5'-TTCTGCCAAAACCACACTTG-3' (WT/KO). Studies on mice were performed at the Charité Universitätsmedizin Berlin approved by the Animal Care and Use Committee from Berlin:LAGeSo. The study using Mg^{2+} diets in *Cnnm2*^{+/+} and *Cnnm2*^{+/-} mice was performed at the Radboud Institute for Molecular Life Sciences, Nijmegen, the Netherlands. The study was ethically approved by the Local Ethical Committee of the Radboud University Nijmegen (RU DEC 2015-0112) and by the Dutch Central Commission for Animal Experiments (CCD, AVD103002016382). This study was performed in compliance with the ARRIVE guidelines.

Experimental design Mg^{2+} diet intervention. Mice were held in standard cages with bedding and kept in a temperature- and light-controlled room. Standard pellet chow and autoclaved tap water were available ad libitum. After genotyping, 36 *Cnnm2*^{+/-} mice and 30 *Cnnm2*^{+/+} (wild-type) mice of age week 8–10 were evenly divided between females and males, and blood was drawn via submandibular puncture. The mice were then kept in metabolic cages individually for 48 h. Faeces and urine were sampled for 24 h. By genotype and sex, mice were subsequently randomly divided in three diet groups, fed with low 0.02% (w/w) Mg^{2+} , normal 0.23% (w/w) Mg^{2+} , or enriched 0.48% Mg^{2+} (w/w) diets. After two weeks, mice were housed again in metabolic cages for faeces and urine sampling for 48 h in total and subsequently euthanised by cervical dislocation under 5% (v/v) isoflurane anaesthesia, followed by dissecting the organs.

Electrolyte measurements. Serum Mg^{2+} and Ca^{2+} concentration of newborn animals were determined by colorimetric assays (QuantiChrom, BioAssay Systems, USA) according to the manufacturer's instruction).

The total Mg^{2+} concentration in serum, urine, and faeces in adult mice was determined by a xylydyl blue colorimetric assay kit according to the manufacturer's protocol (Roche/Hitachi, Japan) and measured at 600 nm on a BioRad plate reader (BioRad, California, USA). Total Ca^{2+} was measured using an o-cresolphthalein complexone method and read at 570 nm, as described previously²². Faeces were dissolved in nitric acid (>65%) and incubated at 65 °C for 15 min prior to measurements. Sodium and potassium were determined by the Radboudumc clinical lab using an automated analysis system (Abbott Diagnostics, the Netherlands).

Antibodies. The hexa-His-tagged intracellular carboxyterminus of murine CNNM2 (aa 593-875) was expressed in BL-21 bacteria and purified using a Nickel-nitrilotriacetic acid-column (QIAGEN, Germany). The hexa-His-tag was removed by cleavage with Tobacco Etch Virus protease (Genscript, the Netherlands). Guinea pigs were immunized with the purified protein (Pineda, Germany). Serum was collected after 60 days and 3 boosts and purified by affinity chromatography using the carboxy-terminus of murine CNNM2. Rabbit anti-NCC was a kind gift from Dr. D.H. Ellison. For western blot analyses, rabbit anti- β -actin (A2228, Sigma-Aldrich, USA) and rabbit anti-CNNM2 (ab111351, Abcam, UK) were used.

SDS-PAGE and Western blot analysis. Tissues were homogenised in 140 mmol/L NaCl, 20 mmol/L Tris, 5 mmol/L EDTA, adjusted with Tris to pH 7.4, with protease inhibitors by Ultra Turrax-T25 followed by

Dounce homogeniser. Samples were centrifuged 10 min 1000 g at 4 °C to remove nuclei. Membranes were pelleted by centrifugation at 100,000 g at 4 °C for 30 min and resuspended in lysis buffer (50 mmol/L Tris-HCl pH 6.8, 5 mmol/L EDTA, 2% (w/v) SDS, with protease inhibitors). For SDS-PAGE, 25 µg protein was loaded, followed by transfer to a polyvinylidene fluoride membrane. Membranes were blocked with 5% (w/v) non-fat dry milk in phosphate buffered solution (PBS) for 1 h at room temperature (RT) and incubated overnight with blocking buffer supplemented with primary antibody at 4 °C. The next day, membranes were washed with PBS and incubated with appropriate peroxidase-conjugated secondary antibodies (Roche, Mannheim, Germany) and visualized by enhanced chemiluminescence.

Histology. Paraffin-embedded brains from adult mice and E17.5 embryos were processed into 5 µm-thick sections and mounted on slides for Nissl staining. Briefly, slides were deparaffinized in xylene for 10 min followed by 5 min incubation in the graded ethanol series (100, 95, 75, 50%). Slides were incubated in 0.1% (w/v) cresyl violet solution prepared in distilled water for 8 min followed by a 2 min differentiation step in 95% ethanol and dehydrated in 100% ethanol for 2 min. Slides were then cleared in xylene and mounted with permanent mounting medium.

Immunohistochemistry. Kidney cryosections (10 µm) of *Cnnm2*^{+/+} and *Cnnm2*^{-/-} embryos were fixed with 4% (w/v) paraformaldehyde in PBS for 8 min. Blocking was performed in 5% (v/v) donkey serum (Biozol, Germany), 0.3% (v/v) Triton X-100 in PBS for 1 h at RT. Sections were then incubated in blocking solution supplemented with guinea pig anti-CNNM2 antibody (1:500), and rabbit anti-NCC (1:500) at RT for 2.5 h followed by secondary antibody (AlexaFluor488 donkey-anti-rabbit and AlexaFluor594 donkey-anti-guinea-pig (ThermoFisher Scientific, Germany)) incubation for 1 h at RT. Finally, sections were mounted by using ProLong Diamond antifade reagent (Invitrogen, Germany) with DAPI and imaged on Nikon Laser Scanning Microscope A1R (AMBIO core facility, Charité Universitätsmedizin, Berlin, Germany).

RNA isolation and real-time quantitative polymerase chain reaction (RT-qPCR). Total RNA was isolated from kidneys and colon using TriZol (Invitrogen, the Netherlands) and treated with DNase (1 U/µg RNA, Promega, USA) Subsequently, cDNA was synthesised from 1.5 µg total RNA by Moloney Murine Leukaemia Virus reverse transcriptase (Invitrogen) at 37 °C for 1 h. IQ SYBR Green Mix (Bio-Rad) was used to determine gene expression levels. Relative expression was determined by the Livak method and shown as fold-change compared to the control group (wild-type mice, 0.23% (w/w) Mg²⁺ diet) and corrected for *Gapdh* expression. All primers used for gene expression analysis were equally efficient (see Supplementary Table 1 for primer sequences).

Structural analysis by the microcomputed tomography. Femurs were dissected and fixed in 4% (v/v) formalin for 24 h and subsequently kept in 70% (v/v) ethanol. Femurs were scanned using the Skyscan 1076 in vivo X-ray computed tomography (Bruker microCT, Kontich, Belgium) with a voxel size of 8.88 µm and 2300 ms exposure time in line with the guidelines for the assessment of bone microstructure²³. The following settings were used: X-ray power of 40 kV and tube current of 250 mA. Beam hardening (20%) was reduced using a 1 mm aluminum filter, ring-artefacts was set at 5 and an average of three photos (frame averaging) at each angle (0.8°) were taken to generate the final images. For the analysis of trabecular bone parameters, the distal metaphysis was scanned (a scan area of 1.35 mm from the distal growth plate towards femoral center). Analysis of the cortical bone parameters was performed in the diaphyseal cortex, which comprised a scan area of 0.45 mm in the femoral center. 3D reconstruction and data analysis were performed with using manufacturer-provided software (NRecon, Data viewer, CT analyzer; Bruker microCT).

Statistics. Data is represented as mean ± SEM. Comparisons were made by a One- or Two-way ANOVA, followed by a Tukey's post-hoc test. An alpha of *P* < 0.05 was considered statistically significant. Statistical analysis is described in detail in the figure legends.

Results

***Cnnm2*^{-/-} mice are embryonically lethal and display exencephaly.** *Cnnm2*^{-/-} mice were developed using CRISPR/Cas9 technology. In a first approach using Cas9 and a single guideRNA (sgRNA), deletions were introduced in exon 1 of the *Cnnm2* locus. Two independent lines were established with either a deletion of 55 bp resulting in a frameshift at position 28 (p.A28D fsX9) or a deletion of 37 bp resulting in a frameshift at position 40 (p.V40H fsX3) (Fig. 1A). In a second approach using Cas9, two sgRNAs and a donor plasmid, LoxP sites were introduced upstream and downstream of exon 1, which was removed by cre mediated excision after crossing the mice with the floxed allele to a cre deleter strain (Fig. 1B). At E18, embryos were present at Mendelian ratio (*Cnnm2*^{+/+}: 27%, *Cnnm2*^{+/-}: 49% *Cnnm2*^{-/-}: 24%) (Fig. 1C). However, the *Cnnm2*^{-/-} offspring all died within the first day after birth in the three investigated lines. Consequently, *Cnnm2*^{-/-} animals were analysed at embryonic day 18 (E18). 36% of *Cnnm2*^{-/-} embryos displayed exencephaly, which may contribute to the mortality of these mice (Fig. 1D,E). The *Cnnm2*^{-/-} embryos (E17.5) that did not show exencephaly also did not show obvious morphological neurological differences, as demonstrated with a Nissl staining (Fig. 1F). Both lines were used to generate mice homozygous for the deleted *Cnnm2* allele and resulted in early postnatal lethality and a similar penetrance of exencephaly.

Absence of CNNM2 protein was confirmed by Western blot analysis of embryonic brains and specificity of the antibody was confirmed using CNNM2 overexpressing Madin-Darby canine kidney (MDCK) cells (Fig. 1G). In

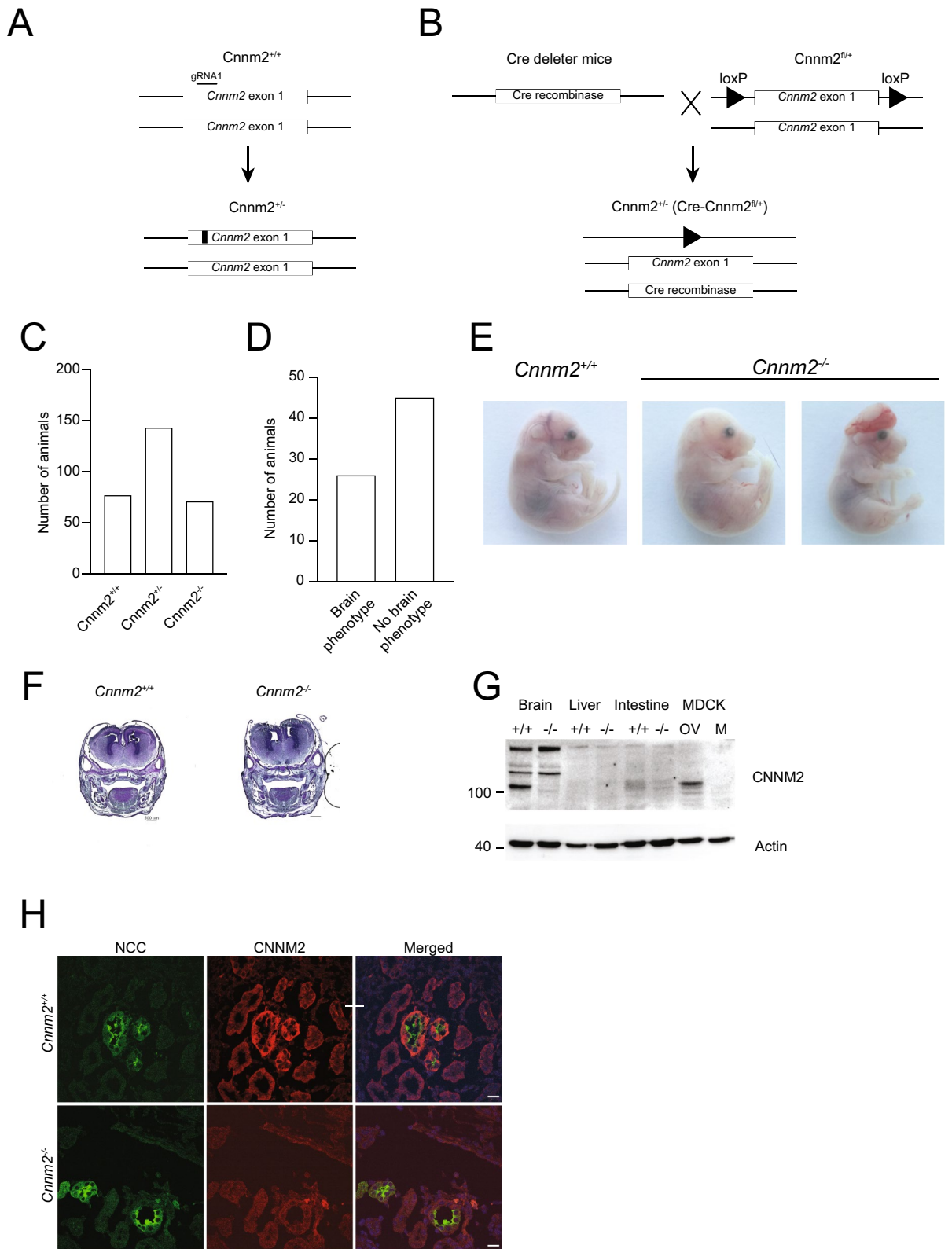


Figure 1. Generation and verification of a *Cnmm2* knock-out mouse model. Schematic overview of the strategy used for genomic deletion of *Cnmm2* by CRISPR/Cas9 mediated deletions (A) or by CRISPR/Cas9 mediated insertion of loxP sites followed by Cre recombinase mediated excision (B). (C) Distribution of the genotype of embryos at E18.5. (D) Distribution of *Cnmm2*^{-/-} mice exhibiting exencephaly. (E) Representative pictures of embryos at E18.5, in which exencephaly is observed in *Cnmm2*^{-/-} mice. (F) Van Nissl staining of E17.5 *Cnmm2*^{+/+} and *Cnmm2*^{-/-} embryos showing no apparent differences in morphology in the absence of exencephaly. (G) Western blot of brain membrane preparation from *Cnmm2*^{+/+} and *Cnmm2*^{-/-} mice. Madin-Darby canine kidney cells transfected with murine *Cnmm2* (OV) or mock (M) served as a control for antibody specificity. (H) Immunohistochemistry of kidney cryo-sections of E18.5 *Cnmm2*^{+/+} and *Cnmm2*^{-/-} stained for CNNM2 (red) and Na⁺/Cl⁻ co-transporter (NCC) (green). Scale bar depicts 50 μm.

addition, immunohistochemistry verified that CNNM2 expression in the DCT, defined by Na^+/Cl^- co-transporter (NCC) positive tubules, was absent in kidney sections of *Cnnm2*^{-/-} pups (Fig. 1H).

***Cnnm2*^{+/-} mice exhibit low serum Mg^{2+} levels.** To determine the effects of CNNM2 depletion on electrolyte homeostasis, serum Mg^{2+} and Ca^{2+} levels were determined in pups within the first hours of life (≤ 8 h). The *Cnnm2*^{-/-} mice had a significant decreased serum Mg^{2+} concentration compared to both *Cnnm2*^{+/-} mice and *Cnnm2*^{+/+} mice (0.68 ± 0.05 mmol/L versus 0.92 ± 0.02 mmol/L and 1.00 ± 0.02 mmol/L, respectively, $P < 0.05$) (Fig. 2A). Determination of the serum Ca^{2+} levels revealed a significant 50% increase in *Cnnm2*^{-/-} mice whereas similar Ca^{2+} levels were observed in *Cnnm2*^{+/-} mice (Fig. 2B).

As *Cnnm2*^{-/-} mice died shortly after birth, further studies to determine the role of CNNM2 in Mg^{2+} homeostasis were performed in the adult *Cnnm2*^{+/-} mice. Adult *Cnnm2*^{+/-} had comparable brain morphology with wild type mice (Supplementary Fig. 2).

To delineate the role of CNNM2 in Mg^{2+} further, *Cnnm2*^{+/+} and *Cnnm2*^{+/-} adult mice were fed with a low, normal, or high Mg^{2+} diet for two weeks (Fig. 2C). Similar to newborn *Cnnm2*^{-/-} mice, adult *Cnnm2*^{+/-} mice displayed significantly decreased Mg^{2+} levels in the blood compared to *Cnnm2*^{+/+} mice (1.05 ± 0.02 versus 1.23 ± 0.02 mmol/L, respectively, $P < 0.05$) (Fig. 2D). When exposed to a low, normal, or high Mg^{2+} diet for two weeks, serum Mg^{2+} levels were consistently low post-diet in *Cnnm2*^{+/-} mice compared to *Cnnm2*^{+/+} (Fig. 2E). No differences were observed in weight gain between mice of different genotypes or when fed on a particular diet (Table 1). In adult *Cnnm2*^{+/-} mice, a slight increase of serum Ca^{2+} concentration was measured compared to *Cnnm2*^{+/+} mice (Fig. 2F,G). Blood Na^+ and K^+ levels remained unaffected upon exposure to the diets (Fig. 2H,I).

***Cnnm2* deficiency leads to mild urinary Mg^{2+} wasting.** To pinpoint the cause of the low serum Mg^{2+} levels in the *Cnnm2*^{+/-} mice, the 24 h urinary Mg^{2+} excretion and kidney mRNA expression of genes involved in Mg^{2+} reabsorption were assessed. Morphology of the kidneys was similar in both genotypes (Fig. 3A). *Cnnm2*^{+/-} deficient mice did not show a significant decrease in urinary Mg^{2+} excretion (38 ± 3.2 versus 37 ± 3.0 mmol/L/24hrs, respectively) in the urine compared to wild type mice across the different diets (Fig. 3B,C), despite having decreased serum Mg^{2+} concentration, suggestive for a small renal reabsorption defect. Interestingly, *Cnnm2*^{+/-} displayed Ca^{2+} retention at the baseline urine measurement (1.0 ± 0.1 vs 1.7 ± 0.1 $\mu\text{mol}/24\text{hrs}$, respectively, $P < 0.0001$) (Fig. 3D), although this effect was not observed at the final day of the diets (Fig. 3E). Gene expression analysis showed significantly decreased renal expression of *Cnnm2* in *Cnnm2*^{+/-} mice on the control and high Mg^{2+} diet (Fig. 3F). Expression of the family member *Cnnm4* was decreased 3.6-fold in *Cnnm2*^{+/-} mice fed on the normal Mg^{2+} -diet (Fig. 3G). Levels of magnesiotropic genes *Trpm6*, *Trpm7*, *Slc41a1* were measured in the kidney, but did not show any genotype-specific effect (Fig. 3H–J). The expression of the epithelial Ca^{2+} channel *Trpv5* showed an overall significant increase due the diets, but no differences were observed between the *Cnnm2*^{+/-} compared to wild type mice (Fig. 3K).

***Cnnm2*^{+/-} mice have perturbed intestinal Mg^{2+} absorption.** Before the start of the diets *Cnnm2*^{+/-} mice displayed a 17.5% higher faecal Mg^{2+} content compared to *Cnnm2*^{+/+} mice (Fig. 4A,B). This was similar to Ca^{2+} levels, which were also significantly increased (Fig. 4C,D). Furthermore, we investigated the mRNA expression of key magnesiotropic genes present in the distal part of the colon, where transcellular Mg^{2+} absorption takes place. Similar to the observation in the kidney, *Cnnm2* transcript levels were significantly reduced in the *Cnnm2*^{+/-} mice compared to control mice. Yet there was an overall increase of *Trpm6* expression and *Cnnm4* expression based on diet or genotype, respectively (Two-Way ANOVA). No diet or genotype dependent changes were observed for other magnesiotropic genes (Fig. 4E–I). The expression of the epithelial Ca^{2+} channel *Trpv6* was not significantly different among all mice groups (Fig. 4J).

***Cnnm2*^{+/-} mice display normal bone morphology.** The femurs of three male mice were subjected to micro-computed tomography analysis. Both the cortical and trabecular bone microarchitecture were not significantly affected by genotype nor diet, except in *Cnnm2*^{+/-} mice on a low Mg^{2+} diet (Fig. 5A–E).

Discussion

In this study, we used several genetic mouse models to investigate the role of CNNM2 in mice. *Cnnm2*^{-/-} mice exhibited maldevelopment of the brain, prominently consisting of exencephaly. The *Cnnm2*^{-/-} newborns displayed hypomagnesaemia concomitant with increased serum Ca^{2+} levels. *Cnnm2*^{+/-} adult mice showed a normal development, but similarly suffered from a low serum Mg^{2+} concentration, which could be partially explained by faecal and renal Mg^{2+} loss. Our study emphasises the role of CNNM2 in embryonic development and overall Mg^{2+} handling, and disclosed a novel role in intestinal Mg^{2+} absorption.

Impaired renal Mg^{2+} reabsorption and urinary Mg^{2+} wasting have been considered as the primary defect of HSMR patients as renal Mg^{2+} excretion remains similar despite lowered serum Mg^{2+} levels^{13,14}. In line with the observation in patients, *Cnnm2*^{+/-} mice displayed low serum Mg^{2+} levels when compared to *Cnnm2*^{+/+} mice. Yet, no significant increase in urinary Mg^{2+} excretion was observed. The *Cnnm2*^{+/-} mice displayed lowered urinary Mg^{2+} excretion upon exposure to lowered Mg^{2+} diet, similarly to wild type mice. This demonstrates the compensatory capacity of Mg^{2+} reabsorption in these mice. Yet, *Cnnm2*^{+/-} mice showed decreased serum Mg^{2+} levels. The fact that this low serum value is not associated with a diminished urinary Mg^{2+} excretion can be interpreted as a sign of a renal Mg^{2+} leak. This has previously been reported in other mouse models of hypomagnesemia, e.g. *Slc41a3*^{-/-} mice and high-fat diet-fed mice^{24,25}. The role of CNNM2 in the kidney has been substantiated by studies of kidney-specific knockout mice of *Cnnm2* which suffer from hypomagnesemia, demonstrating that CNNM2 regulates renal Mg^{2+} handling¹⁹.

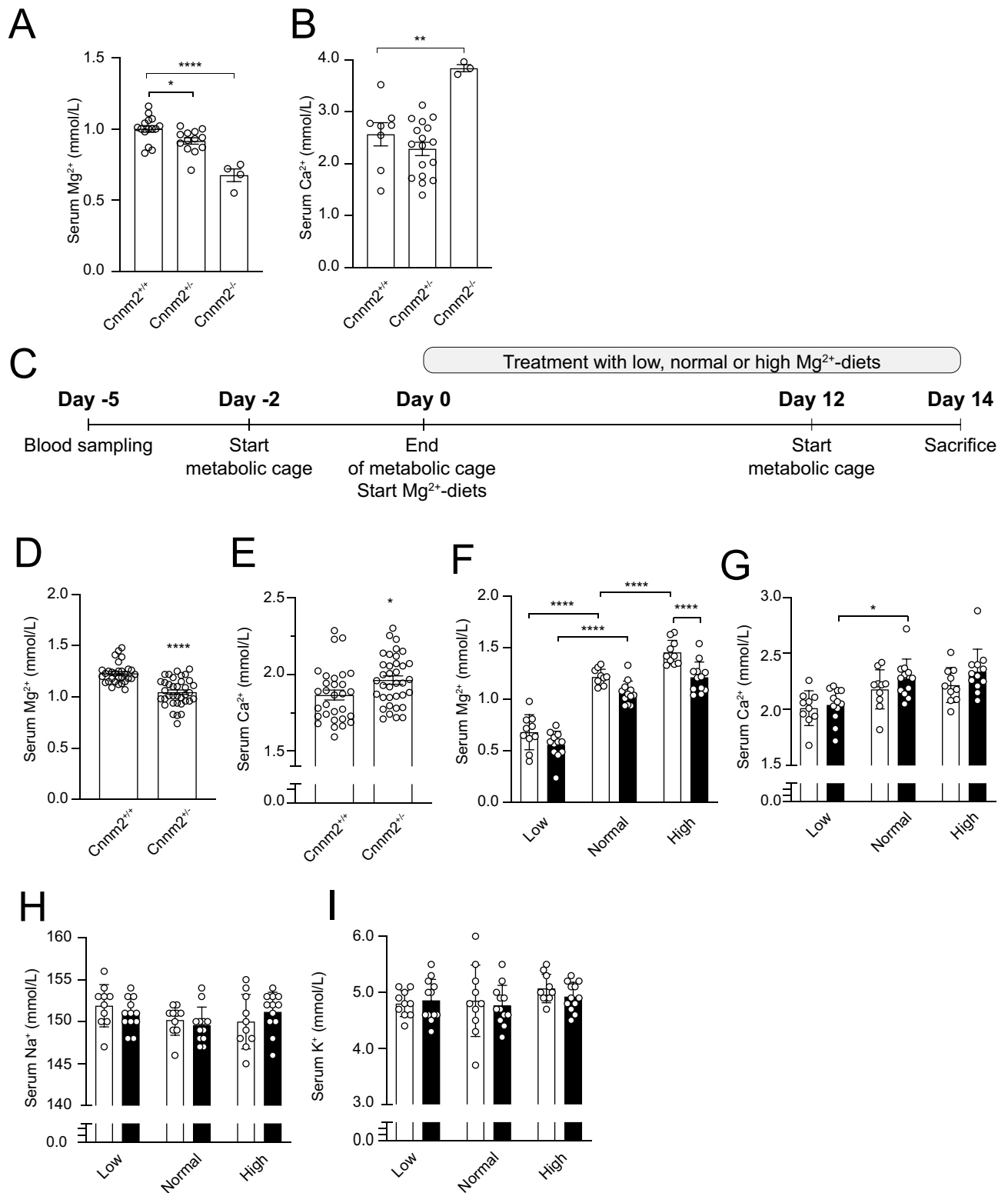


Figure 2. CNNM2 depletion affects Mg²⁺ and Ca²⁺ homeostasis. (A) Serum Mg²⁺ is significantly reduced in newborn CNNM2 deficient mice compared to wild type littermates. Data are presented as mean ± SEM (n = 4–15) (B) Serum Ca²⁺ in newborn *Cnnm2*^{-/-} mice is significantly increased compared to *Cnnm2*^{+/+} mice (n = 3–17) (C) *Cnnm2*^{+/+} or *Cnnm2*^{-/-} mice were treated with low (0.02%), normal (0.23%), or high (0.48%) (w/w) Mg²⁺ diets for two weeks, followed by housing in metabolic cages. (D,F) *Cnnm2*^{+/-} mice (black bars) have lower serum Mg²⁺ levels and higher compared to wild type mice (white bars), independent of the Mg²⁺ diet. (E,G) *Cnnm2*^{+/-} mice have lower serum Mg²⁺ levels and an overall increase in serum Ca²⁺ levels compared to wild type littermates, independent of the Mg²⁺ diet. Serum Na⁺ (H) and K⁺ (I) levels in *Cnnm2*^{+/-} mice are unchanged (n = 10–12 per group). Data are presented as mean ± SEM. Significance determined with two-tailed Student's T-test or Two-way ANOVA followed by a Tukey post-hoc test. **p* < 0.05, ***p* < 0.01, ****p* < 0.001, *****p* < 0.0001.

Diet	<i>Cnnm2</i> ^{+/+}			<i>Cnnm2</i> ^{-/-}		
	Low	Normal	High	Low	Normal	High
Body weight M (g)	23.7 ± 0.3	22.8 ± 0.3	24.4 ± 0.3	23.3 ± 0.4	23.7 ± 0.8	23.7 ± 0.5
Body weight F (g)	19.5 ± 0.8	19.5 ± 0.5	19.7 ± 0.4	20.1 ± 0.4	20.3 ± 0.2	20.7 ± 0.3
Food intake (g)	3.5 ± 0.1	3.0 ± 0.2	3.4 ± 0.2	3.5 ± 0.2	3.5 ± 0.2	3.2 ± 0.3
Water intake (mL)	10 ± 2.4	9.7 ± 1.8	10 ± 1.7	10 ± 1.6	10 ± 1.3	7.9 ± 0.9
Urine excretion (mL/24 h)	3.4 ± 0.9	2.3 ± 0.4	3.8 ± 0.7	3.7 ± 0.7	3.3 ± 0.4	3.5 ± 0.6
Faecal (mg/24 h)	384 ± 21	429 ± 40	450 ± 36	391 ± 40	442 ± 38	428 ± 35

Table 1. Metabolic parameters of *Cnnm2*^{+/+} mice upon exposure to different Mg²⁺ diets. *Cnnm2*^{+/+} and *Cnnm2*^{-/-} mice were kept in metabolic cages exposed at low (0.02%), normal (0.21%) and high (0.48%) (w/w) Mg²⁺ diets for 14 days. The last 48 h, mice were kept in metabolic cages for the collection of urine and faeces. Values represent the latter 24 h (mean ± SEM). M male, F female.

Interestingly, intestinal malabsorption may also play a role in the Mg²⁺ deficiency observed in the *Cnnm2*^{-/-} mice. At basal conditions, faecal Mg²⁺ excretion was increased in *Cnnm2*^{-/-} mice, indicative of Mg²⁺ malabsorption. Although CNNM2 has been primarily studied in the kidney, our current and previous studies demonstrate that *Cnnm2* is expressed in the distal colon⁸. Indeed, several recent single cell RNA sequencing datasets in colon and rectum confirm that CNNM2 is particularly expressed in enterocytes^{26,27}. Of interest, CNNM4, a close family member of CNNM2, is present in the basolateral membrane of the colon, where it orchestrates Mg²⁺ efflux^{28–30}. We have previously shown an interaction of CNNM2 with CNNM4 upon expression in HEK293 cells, suggesting that these proteins could form a complex⁸. Indeed, a significant increase of *Cnnm4* expression in the colon was observed in *Cnnm2*^{-/-} mice, suggesting that CNNM4 compensates for the loss of CNNM2. However, a CNNM4-independent function of CNNM2 cannot be excluded. Although malabsorption of Mg²⁺ was not previously reported in *Cnnm2*^{-/-} mice or patients¹⁹, it should be noted that faecal Mg²⁺ excretion is often not detected or even determined in mice, although also in intestinal-specific *Trmp6*^{-/-} and *Trpm7*^{-/-} mice decreased serum Mg²⁺ levels and increased faecal Mg²⁺ excretion can be observed^{6,31}. On average, 30% of dietary Mg²⁺ is absorbed and foremost ends in the faeces, making it challenging to detect changes in absorption. However, Mg²⁺ supplementation was proven difficult in patients with CNNM2 mutations, which potentially indicates a reduced ability to absorb Mg²⁺^{13,14}. Our findings suggest that oral Mg²⁺ supplementation in patient with HSMR syndrome depends on paracellular Mg²⁺ transport in the duodenum, as transcellular Mg²⁺ absorption in the colon may be reduced by CNNM2 mutations.

In addition to the Mg²⁺ disturbances, *Cnnm2*^{-/-} mice displayed renal Ca²⁺ retention resulting in an increased serum Ca²⁺ concentration. Decreased serum Mg²⁺ levels could trigger the TAL to increase its paracellular Mg²⁺ transport. In addition, this would lead to increased Ca²⁺ reabsorption and decreased urinary Ca²⁺ levels, which is coordinated via Claudins 10, 14, 16 and 19^{32–36}. This compensatory capacity may be specific for mice, as patients with mutated CNNM2 have significant urinary Mg²⁺ wasting. In line with this, 24 h urinary Ca²⁺ levels are normal in patients with CNNM2 mutations. Interestingly, a few patients with CNNM2 mutations have been reported with impaired Ca²⁺ and phosphate homeostasis. Whether this is a common phenotype in these patients remains to be determined, as the patients are consanguineous or have other genetic defects, such as mutations in the vitamin D receptor (VDR)^{12,37}. However, the role of TAL in CNNM2-associated physiology should be interpreted with caution, as direct effects of CNNM2 on Ca²⁺ homeostasis cannot be excluded.

Our study demonstrates that CNNM2 is essential for brain development and early life survival. Until embryonic day 18.5, the *Cnnm2*^{-/-} embryos were present at Mendelian ratios, but newborn *Cnnm2*^{-/-} mice died shortly after birth. Although lethality of *Cnnm2*^{-/-} mice was reported earlier¹⁹, we are the first to report the presence of exencephaly, which suggests that neural tube defects contribute to the brain phenotype. It is known that defects in the closure of the cranial neural tube result in protrusion of the neuroepithelium outside the developing brain, inevitably disturbing normal neurodevelopment³⁸. Although previous studies suggested an important role of CNNM2 in brain function, the exact consequences of CNNM2 deficiency may be species-dependent. Patients with recessive CNNM2 mutations exhibit structural brain deformities, such as demyelination, failure of opercularisation, and cerebral cortical atrophy, often concomitant with motor skill defects, epileptic seizures, and intellectual disability^{12,13}. Moreover, knockdown of *cnnm2* in zebrafish resulted in maldevelopment of the mid-hindbrain boundary¹³.

Interestingly, exencephaly and other neural tube defects have been more often observed in mouse models of hypomagnesaemia. *Trmp6* knockout mice display embryonic lethality, which is accompanied by the presence of exencephaly and spina bifida^{5,39}. Similarly, the absence of *Trpm7* expression in mice during embryonic development, a close homologue of TRPM6, has been associated with neural tube defects^{40,41}. Although this homology suggests that neural tube defects may be the direct result of hypomagnesaemia, it should be noted that neural tube defects are uncommon in patients with hypomagnesaemia¹. Consequently, it remains to be determined whether this is a Mg²⁺ dependent or independent effect. Of note: as only a subset of *Cnnm2*^{-/-} mice displayed exencephaly, neural tube defects may only partially explain the lethality.

The absence of a clear urinary Mg²⁺ wasting in *Cnnm2*^{-/-} mice shows that renal Mg²⁺ reabsorption may be different in mice and men, as HSMR syndrome show clear renal Mg²⁺ wasting¹³. In line with this, kidney-specific *Trpm6* knock out mice were reported to have normal serum Mg²⁺ levels and without renal Mg²⁺ leak, unlike patients with *Trpm6* mutations (HOMG1/HSH; MIM# 602014)³¹. Similarly, *Kcnj10* and *Fxyd2* knock out

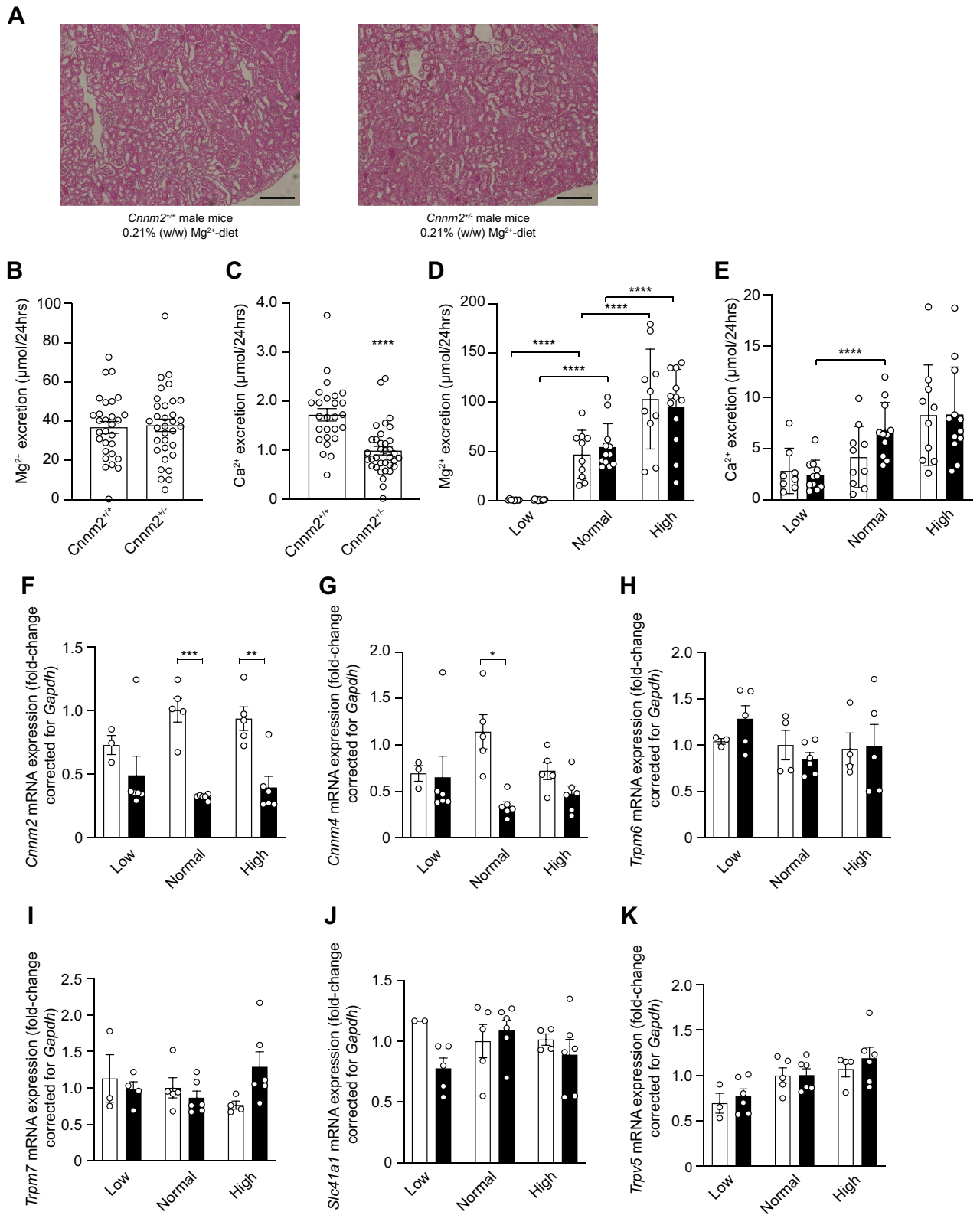


Figure 3. *Cnnm2* deficiency does not affect overall renal Mg^{2+} reabsorption. (A) Representative pictures of kidney morphology by H&E staining. Scale bar depicts 50 μm . (B,D) *Cnnm2*^{+/-} mice do not show altered Mg^{2+} excretion via the urine, but retain more Ca^{2+} ($n = 30-36$ per group). (C-E) Lower Mg^{2+} intake is associated with lower renal Mg^{2+} excretion, not with Ca^{2+} , independent of genotype in *Cnnm2*^{+/-} mice (black bars) ($n = 8-12$ per group). (F) Renal *Cnnm2* expression is lowered in *Cnnm2*^{+/-} mice, *Cnnm4* (G), *Trpm6* (H), *Trpm7* (I), *Slc41a1* (J), and *Trpv5* (K) remain majorly unaltered ($n = 3-6$ mice per group). Data are presented as mean \pm SEM. Significance determined with two-tailed Student's T-test or Two-way ANOVA followed by a Tukey post-hoc test. * $p < 0.05$, ** $p < 0.01$, *** $p < 0.001$, **** $p < 0.0001$.

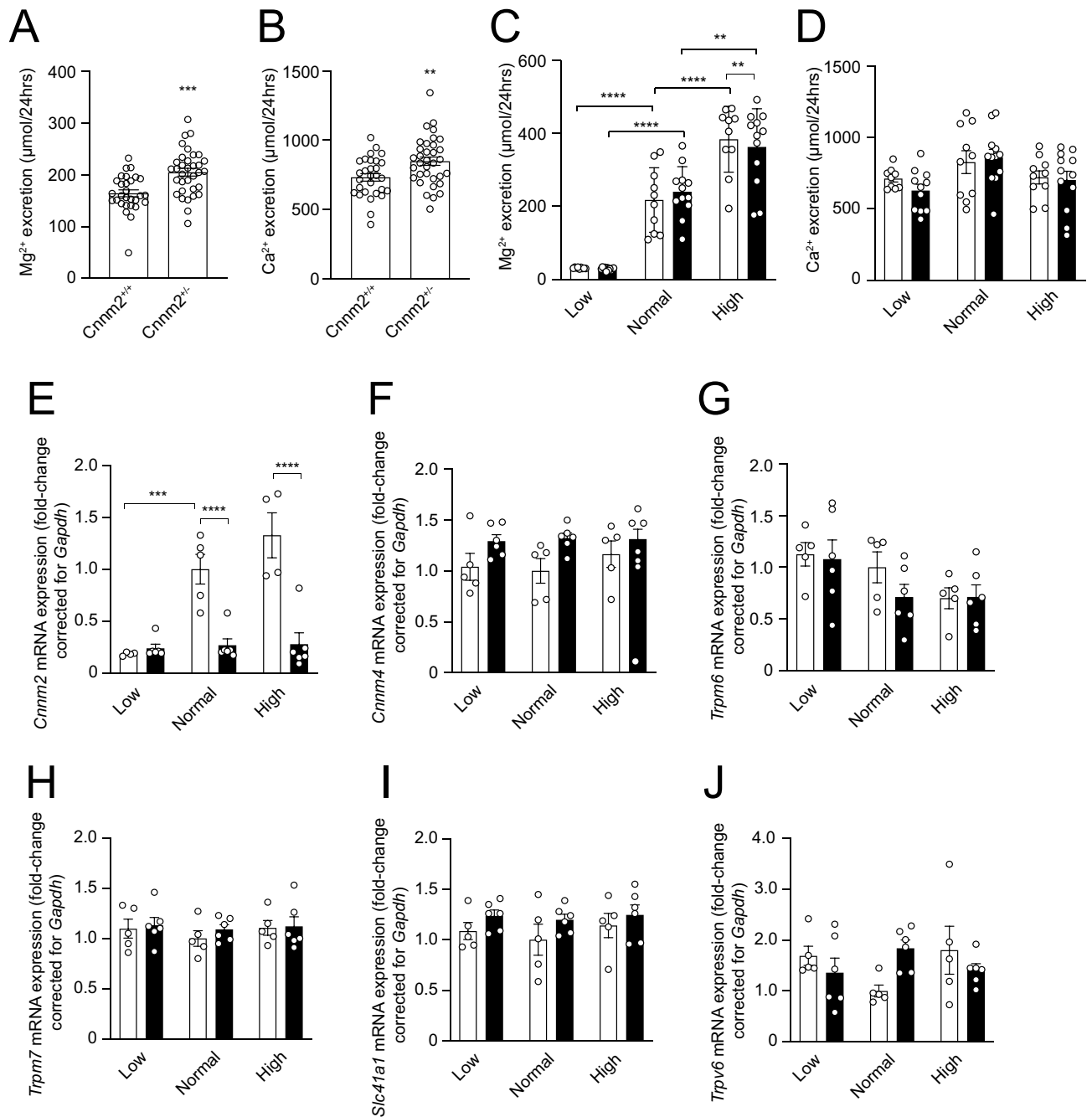


Figure 4. *Cnnm2* deficiency decreases faecal Mg^{2+} absorption. (A,C) *Cnnm2*^{-/-} mice display significantly increased Mg^{2+} and Ca^{2+} excretion via the faeces ($n = 29\text{--}34$ per group). (B,D) Lower Mg^{2+} intake is associated with lower intestinal Mg^{2+} excretion, not with Ca^{2+} , independent of genotype in *Cnnm2*^{+/+} (white bars) and *Cnnm2*^{-/-} mice (black bars) ($n = 8\text{--}12$ per group) (E) *Cnnm2* expression is significantly diminished in *Cnnm2*^{-/-} mice, *Cnnm4* (G), *Trpm6* (H), *Trpm7* (I), *Slc41a1* (J), and *Trpv6* (K) remain unaltered ($n = 3\text{--}6$ per group). Data are presented as mean \pm SEM. Significance determined with two-tailed Student's T-test or Two-way ANOVA followed by a Tukey post-hoc test. * $p < 0.05$, ** $p < 0.01$, *** $p < 0.001$, **** $p < 0.0001$.

animals have normal urinary Mg^{2+} levels, in contrast to patients with mutations (OMIM: 612780 & 154020)^{42–46}. Additionally, a mice model deficient in solute carrier family 41 member 3 (*Slc41a3*) expression, a putative Mg^{2+} transporter and highly enriched in DCT, was associated with hypomagnesemia without renal Mg^{2+} wasting²⁴. Altogether, these studies show that mice are able to compensate better for impaired DCT Mg^{2+} reabsorption compared to men.

In conclusion, CNNM2 regulates the systemic Mg^{2+} balance and is essential for neurodevelopment. Our study points toward a putative role of CNNM2 in intestinal Mg^{2+} absorption.

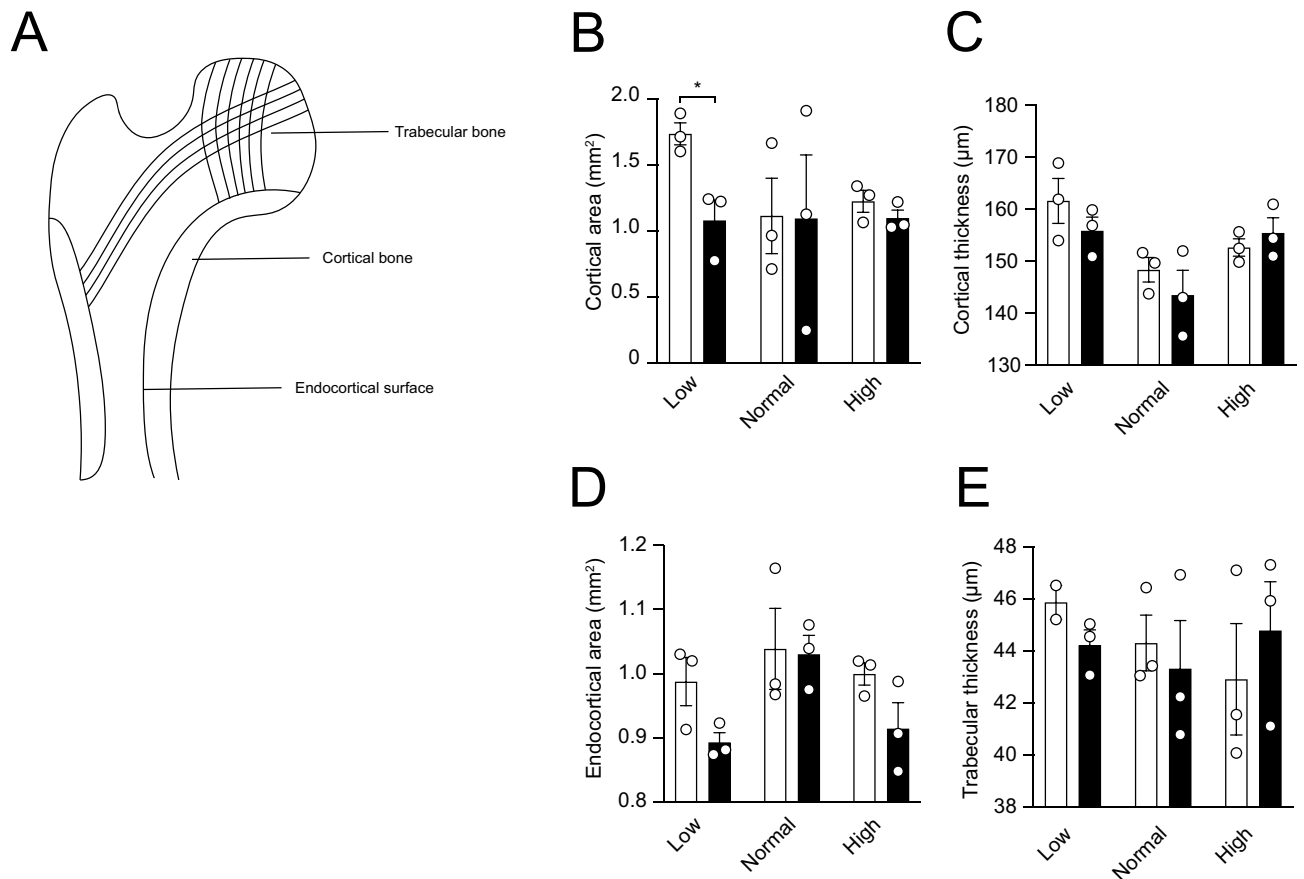


Figure 5. CNNM2 depletion does not affect bone morphology. Micro-CT analysis of femurs of which the cortical area (A) and thickness (B) were determined, endocortical area (C) and trabecular thickness (D). (n = 3 per group) Data are presented as mean \pm SEM. Significance determined with two-tailed Student's T-test or Two-way ANOVA followed by a Tukey post-hoc test. * $p < 0.05$.

Received: 28 November 2020; Accepted: 26 March 2021

Published online: 15 April 2021

References

- de Baaij, J. H., Hoenderop, J. G. & Bindels, R. J. Magnesium in man: implications for health and disease. *Physiol. Rev.* **95**(1), 1–46 (2015).
- Quamme, G. A. & Dirks, J. H. Magnesium transport in the nephron. *Am. J. Physiol.* **239**(5), F393–401 (1980).
- Groenestege, W. M. *et al.* The epithelial Mg²⁺ channel transient receptor potential melastatin 6 is regulated by dietary Mg²⁺ content and estrogens. *J. Am. Soc. Nephrol.* **17**(4), 1035–1043 (2006).
- Thebault, S. *et al.* EGF increases TRPM6 activity and surface expression. *J. Am. Soc. Nephrol.* **20**(1), 78–85 (2009).
- Woudenberg-Vrenken, T. E. *et al.* Transient receptor potential melastatin 6 knockout mice are lethal whereas heterozygous deletion results in mild hypomagnesemia. *Nephron Physiol.* **117**(2), 11–19 (2011).
- Mittermeier, L. *et al.* TRPM7 is the central gatekeeper of intestinal mineral absorption essential for postnatal survival. *Proc. Natl. Acad. Sci.* **116**(10), 4706–4715 (2019).
- Li, M., Jiang, J. & Yue, L. Functional characterization of homo- and heteromeric channel kinases TRPM6 and TRPM7. *J. Gen. Physiol.* **127**(5), 525–537 (2006).
- de Baaij, J. H. F. *et al.* Membrane topology and intracellular processing of cyclin M2 (CNNM2). *J. Biol. Chem.* **287**(17), 13644–13655 (2012).
- Arjona, F. J. & de Baaij, J. H. F. CrossTalk opposing view: CNNM proteins are not Na⁽⁺⁾/Mg⁽²⁺⁾ exchangers but Mg⁽²⁺⁾ transport regulators playing a central role in transepithelial Mg⁽²⁺⁾ (re)absorption. *J. Physiol.* **596**(5), 747–750 (2018).
- Arjona, F. J. & de Baaij, J. H. F. Rebuttal from Francisco J. Arjona and Jeroen H. F. de Baaij. *J. Physiol.* **596**(5), 753–754 (2018).
- Sponder, G. *et al.* Human CNNM2 is not a Mg⁽²⁺⁾ transporter per se. *Pflugers Arch.* **468**(7), 1223–1240 (2016).
- Accogli, A. *et al.* CNNM2 homozygous mutations cause severe refractory hypomagnesemia, epileptic encephalopathy and brain malformations. *Eur. J. Med. Genet.* **62**(3), 198–203 (2019).
- Arjona, F. J. *et al.* CNNM2 mutations cause impaired brain development and seizures in patients with hypomagnesemia. *PLoS Genet.* **10**(4), e1004267 (2014).
- Stuiver, M. *et al.* CNNM2, encoding a basolateral protein required for renal Mg²⁺ handling, is mutated in dominant hypomagnesemia. *Am. J. Hum. Genet.* **88**(3), 333–343 (2011).
- Li, C. *et al.* Genome-wide association study meta-analysis of long-term average blood pressure in East Asians. *Circ. Cardiovasc. Genet.* **10**(2), e001527–e001527 (2017).
- Ly, W.-Q. *et al.* Novel common variants associated with body mass index and coronary artery disease detected using a pleiotropic cFDR method. *J. Mol. Cell. Cardiol.* **112**, 1–7 (2017).

17. Ohi, K. *et al.* The impact of the genome-wide supported variant in the cyclin M2 gene on gray matter morphology in schizophrenia. *Behav. Brain Funct. BBF* **9**, 40–40 (2013).
18. Rose, E. J. *et al.* Effects of a novel schizophrenia risk variant rs7914558 at CNNM2 on brain structure and attributional style. *Br. J. Psychiatry* **204**(2), 115–121 (2014).
19. Funato, Y., Yamazaki, D. & Miki, H. Renal function of cyclin M2 Mg²⁺ transporter maintains blood pressure. *J. Hypertens.* **35**(3), 585–592 (2017).
20. Wang, H. *et al.* One-step generation of mice carrying mutations in multiple genes by CRISPR/Cas-mediated genome engineering. *Cell* **153**(4), 910–918 (2013).
21. Lorenz, C., Pusch, M. & Jentsch, T. J. Heteromultimeric CLC chloride channels with novel properties. *Proc. Natl. Acad. Sci. U. S. A.* **93**(23), 13362–13366 (1996).
22. Hoenderop, J. G. J. *et al.* Calcitriol controls the epithelial calcium channel in kidney. *J. Am. Soc. Nephrol.* **12**(7), 1342 (2001).
23. Bouxsein, M. L. *et al.* Guidelines for assessment of bone microstructure in rodents using micro-computed tomography. *J. Bone Miner. Res.* **25**(7), 1468–1486 (2010).
24. de Baaij, J. H. *et al.* Identification of SLC41A3 as a novel player in magnesium homeostasis. *Sci. Rep.* **6**, 28565 (2016).
25. Kurstjens, S. *et al.* Renal phospholipidosis and impaired magnesium handling in high-fat-diet-fed mice. *FASEB J.* **33**(6), 7192–7201 (2019).
26. Parikh, K. *et al.* Colonic epithelial cell diversity in health and inflammatory bowel disease. *Nature* **567**(7746), 49–55 (2019).
27. Wang, Y. *et al.* Single-cell transcriptome analysis reveals differential nutrient absorption functions in human intestine. *J. Exp. Med.* **217**(2) (2019).
28. Funato, Y. *et al.* Membrane protein CNNM4-dependent Mg²⁺ efflux suppresses tumor progression. *J. Clin. Investig.* **124**(12), 5398–5410 (2014).
29. Yamazaki, D. *et al.* Cnnm4 deficiency suppresses Ca²⁺ signaling and promotes cell proliferation in the colon epithelia. *Oncogene* **38**(20), 3962–3969 (2019).
30. Yamazaki, D. *et al.* Basolateral Mg²⁺ extrusion via CNNM4 mediates transcellular Mg²⁺ transport across epithelia: a mouse model. *PLoS Genet.* **9**(12), e1003983 (2013).
31. Chubanov, V. *et al.* Epithelial magnesium transport by TRPM6 is essential for prenatal development and adult survival. *Elife* **5**, e20914 (2016).
32. Breiderhoff, T. *et al.* Deletion of claudin-10 (Cldn10) in the thick ascending limb impairs paracellular sodium permeability and leads to hypermagnesemia and nephrocalcinosis. *Proc. Natl. Acad. Sci. U. S. A.* **109**(35), 14241–14246 (2012).
33. Dimke, H. *et al.* Activation of the Ca(2+)-sensing receptor increases renal claudin-14 expression and urinary Ca(2+) excretion. *Am. J. Physiol. Renal Physiol.* **304**(6), F761–F769 (2013).
34. Gong, Y. *et al.* Claudin-14 regulates renal Ca⁺⁺ transport in response to CaSR signalling via a novel microRNA pathway. *Embo J.* **31**(8), 1999–2012 (2012).
35. Hou, J. *et al.* Claudin-16 and claudin-19 interaction is required for their assembly into tight junctions and for renal reabsorption of magnesium. *Proc. Natl. Acad. Sci. U. S. A.* **106**(36), 15350–15355 (2009).
36. Ohta, H. *et al.* Restricted localization of claudin-16 at the tight junction in the thick ascending limb of Henle's loop together with claudins 3, 4, and 10 in bovine nephrons. *J. Vet. Med. Sci.* **68**(5), 453–463 (2006).
37. García-Castaño, A. *et al.* Novel variant in the CNNM2 gene associated with dominant hypomagnesemia. *PLoS ONE* **15**(9), e0239965 (2020).
38. Copp, A. J. & Greene, N. D. E. Neural tube defects—disorders of neurulation and related embryonic processes. *Wiley Interdiscip. Rev. Dev. Biol.* **2**(2), 213–227 (2013).
39. Walder, R. Y. *et al.* Mice defective in Trpm6 show embryonic mortality and neural tube defects. *Hum. Mol. Genet.* **18**(22), 4367–4375 (2009).
40. Jin, J. *et al.* The channel kinase, TRPM7, is required for early embryonic development. *Proc. Natl. Acad. Sci. U. S. A.* **109**(5), E225–E233 (2012).
41. Liu, W. *et al.* TRPM7 regulates gastrulation during vertebrate embryogenesis. *Dev. Biol.* **350**(2), 348–357 (2011).
42. Reichold, M. *et al.* KCNJ10 gene mutations causing EAST syndrome (epilepsy, ataxia, sensorineural deafness, and tubulopathy) disrupt channel function. *Proc. Natl. Acad. Sci. U. S. A.* **107**(32), 14490–14495 (2010).
43. Arystarkhova, E. *et al.* Paradoxical activation of the sodium chloride cotransporter (NCC) without hypertension in kidney deficient in a regulatory subunit of Na, K-ATPase, FXYD2. *Physiol. Rep.* **2**(12), e12226 (2014).
44. de Baaij, J. H. *et al.* Recurrent FXYD2 p.Gly41Arg mutation in patients with isolated dominant hypomagnesaemia. *Nephrol. Dial. Transplant.* **30**(6), 952–957 (2015).
45. Jones, D. H. *et al.* Na, K-ATPase from mice lacking the gamma subunit (FXYD2) exhibits altered Na⁺ affinity and decreased thermal stability. *J. Biol. Chem.* **280**(19), 19003–19011 (2005).
46. Meij, I. C. *et al.* Dominant isolated renal magnesium loss is caused by misrouting of the Na(+), K(+)-ATPase gamma-subunit. *Nat. Genet.* **26**(3), 265–266 (2000).

Acknowledgements

This work was financially supported by grants from the Netherlands Organization for Scientific Research (NWO Veni 016.186.012, Vici 016.130.668), and the European Joint Program for Rare Diseases (EJPRD2019-40). M.S. and D.M. were supported by the Deutsche Forschungsgemeinschaft (DFG), Research Training Group GRK 2318.

Author contributions

G.F., M.S., C.B., R.B., J.H., D.M., T.B., and J.d.B. designed the research studies, G.F., M.S., C.B., L.S., T.B., and J.d.B. conducted experiments and/or analysed data, G.F. and J.d.B. wrote the manuscript. All authors corrected the manuscript and approved the final version.

Competing interests

The authors declare no competing interests.

Additional information

Supplementary Information The online version contains supplementary material available at <https://doi.org/10.1038/s41598-021-87548-6>.

Correspondence and requests for materials should be addressed to J.H.F.B.

Reprints and permissions information is available at www.nature.com/reprints.

Publisher's note Springer Nature remains neutral with regard to jurisdictional claims in published maps and institutional affiliations.



Open Access This article is licensed under a Creative Commons Attribution 4.0 International License, which permits use, sharing, adaptation, distribution and reproduction in any medium or format, as long as you give appropriate credit to the original author(s) and the source, provide a link to the Creative Commons licence, and indicate if changes were made. The images or other third party material in this article are included in the article's Creative Commons licence, unless indicated otherwise in a credit line to the material. If material is not included in the article's Creative Commons licence and your intended use is not permitted by statutory regulation or exceeds the permitted use, you will need to obtain permission directly from the copyright holder. To view a copy of this licence, visit <http://creativecommons.org/licenses/by/4.0/>.

© The Author(s) 2021